

The O IV and S IV intercombination lines in the ultraviolet spectra of astrophysical sources

F.P. Keenan¹, S. Ahmed¹, T. Brage², J.G. Doyle³, B.R. Espey⁴, K.M. Exter⁵, A. Hibbert⁶, M.T.C. Keenan⁷, M.S. Madjarska³, M. Mathioudakis¹ and D.L. Pollacco¹

¹*Department of Pure and Applied Physics, Queen's University, Belfast BT7 1NN*

²*Kurslab LU, Department of Physics, University of Lund, S-221 00, Lund, Sweden*

³*Armagh Observatory, Armagh BT61 9DG*

⁴*Physics Department, Trinity College Dublin, Dublin 2, Ireland*

⁵*School of Cosmic Physics, Dublin Institute for Advanced Studies, 5 Merrion Square, Dublin 2, Ireland*

⁶*Department of Applied Mathematics and Theoretical Physics, Queen's University, Belfast BT7 1NN*

⁷*Hazelwood College, 70 Whitewell Road, Belfast BT36 7ES*

Abstract.

New electron density diagnostic line ratios are presented for the O IV $2s^2 2p^2 \ ^2P-2s2p^2 \ ^4P$ and S IV $3s^2 3p^2 \ ^2P-3s3p^2 \ ^4P$ intercombination lines around 1400 Å. A comparison of these with observational data for the symbiotic star RR Telescopii (RR Tel), obtained with the *Space Telescope Imaging Spectrograph* (STIS), reveals generally very good agreement between theory and observation. However the S IV $^2P_{3/2}-^4P_{1/2}$ transition at 1423.824 Å is found to be blended with an unknown feature at 1423.774 Å. The line width for the latter indicates that the feature arises from a species with a large ionization potential. In addition, the S IV $^2P_{1/2}-^4P_{3/2}$ transition at 1398.044 Å is identified for the first time (to our knowledge) in an astrophysical source other than the Sun, and an improved wavelength of 1397.166 Å is measured for the O IV $^2P_{1/2}-^4P_{3/2}$ line. The O IV and S IV line ratios in a sunspot plume spectrum, obtained with the *Solar Ultraviolet Measurements of the Emitted Radiation* (SUMER) instrument on the Solar and Heliospheric Observatory, are found to be consistent, and remove discrepancies noted in previous comparisons of these two ions.

Keywords: atomic data — Sun: UV radiation — binaries: symbiotic

1. INTRODUCTION

The O IV $2s^2 2p^2 \ ^2P-2s2p^2 \ ^4P$ and S IV $3s^2 3p^2 \ ^2P-3s3p^2 \ ^4P$ intercombination multiplets around 1400 Å show prominent emission lines in the spectra of the Sun and other astrophysical sources (see, for example, Feldman et al. 1997; Keenan et al. 1993). It has long been known that intensity ratios involving these transitions provide very useful electron density (N_e) diagnostics for the emitting plasma (Flower & Nussbaumer 1975; Bhatia, Doschek & Feldman 1980). However more recently several authors have noted discrepancies between theoretical



© 2002 Kluwer Academic Publishers. Printed in the Netherlands.

line ratios and observational data. For example, Cook et al. (1995) found that the O IV ratios imply densities which differ by up to an order of magnitude, while some observed S IV line ratios lay outside the range of values allowed by theory. Although some of these discrepancies were subsequently resolved by improved atomic data for O IV (Brage, Judge & Brekke 1996), several still remain, such as a disagreement between theory and observation for the I(1397.2 Å)/I(1404.7 Å) intensity ratio in O IV (Harper et al. 1999).

In this paper we use the most up-to-date atomic physics calculations for O IV and S IV to derive intercombination line ratios applicable to a wide range of astrophysical phenomena. These calculations are subsequently compared with high spectral resolution and signal-to-noise observational data, in particular a spectrum of the symbiotic star RR Telescopii (RR Tel) recently obtained with the *Hubble Space Telescope*. The aim of this work is to investigate the accuracy of the O IV and S IV diagnostics, and to assess the importance of possible blending in the observations.

2. ADOPTED ATOMIC DATA AND THEORETICAL LINE RATIOS

The model ion for O IV consisted of the 15 energetically lowest fine-structure levels ($2s^22p^2P_{1/2,3/2}$; $2s2p^2^4P_{1/2,3/2,5/2}$, $^2D_{3/2,5/2}$, 2S , $^2P_{1/2,3/2}$; $2p^3^4S$, $^2D_{3/2,5/2}$, $^2P_{1/2,3/2}$), while that for S IV comprised the lowest 5 levels ($3s^23p^2P_{1/2,3/2}$; $3s3p^2^4P_{1/2,3/2,5/2}$). Energies for these levels were obtained from Safronova, Johnson & Safronova (1996) and Martin, Zalubas & Musgrove (1990) for O IV and S IV, respectively. For both ions, we note that test calculations including higher-lying levels had a negligible effect on the theoretical line ratios considered in this paper.

Electron impact excitation rates for transitions in O IV and S IV were taken from Zhang, Graziani & Pradhan (1994) and Tayal (2000), respectively. Einstein A-coefficients for O IV were obtained from Brage et al. (1996) for $2s^22p-2s2p^2$ transitions, Dankwort & Treffitz (1978) for $2s^22p-2p^3$ and Nussbaumer & Storey (1982) for $2s^22p^2P_{1/2}-2s^22p^2P_{3/2}$. Data for the $3s^23p^2P-3s3p^2^4P$ intercombination lines in S IV were taken from Hibbert, Brage & Fleming (2002), while for all other radiative rates in this ion the calculations of Johnson, Kingston & Dufton (1986) and Bhatia et al. (1980) were adopted. Proton impact excitation rates for O IV were obtained from Foster, Keenan & Reid (1996) and Foster, Reid & Keenan (1997), and those for S IV from Bhatia et al. (1980).

Using the atomic data discussed above in conjunction with the statistical equilibrium code of Dufton (1977), relative O IV and S IV level populations and hence emission line strengths were calculated for a range of electron temperatures (T_e) and densities (N_e). Details of the procedures involved and approximations made may be found in Dufton (1977) and Dufton et al. (1978). Given typical uncertainties in the adopted atomic data of ± 10 per cent (see references above), we would expect our line ratio calculations to be in error by at most ± 15 per cent.

In Figs 1–4 we present O IV and S IV theoretical line intensity ratios generated under two sets of plasma conditions. The first set of results (Figs 1 and 3) are appropriate to solar and stellar transition region observations. These have been calculated at the electron temperatures of maximum O IV and S IV fractional abundances in ionization equilibrium ($\log T_{max}(\text{O IV}) = 5.2$; $\log T_{max}(\text{S IV}) = 5.0$; Mazzotta et al. 1998), plus $\log T_{max} - 0.2$ and $\log T_{max} + 0.2$ for O IV and S IV, respectively, and for electron densities in the range $N_e = 10^8 - 10^{13} \text{ cm}^{-3}$. The second set of theoretical line ratios (Figs 2 and 4) are applicable to observations of gaseous nebulae, and have been calculated at $T_e = 10\,000$ and $20\,000 \text{ K}$, and electron densities between $10^3 - 10^{10} \text{ cm}^{-3}$.

The O IV line intensity ratios in Figs 1 and 2 are
 $R_1 = I(2s^2 2p^2 P_{3/2} - 2s 2p^2^4 P_{1/2}) / I(2s^2 2p^2 P_{3/2} - 2s 2p^2^4 P_{5/2}) = I(1407.3 \text{ \AA}) / I(1401.1 \text{ \AA})$ and
 $R_2 = I(2s^2 2p^2 P_{3/2} - 2s 2p^2^4 P_{1/2}) / I(2s^2 2p^2 P_{3/2} - 2s 2p^2^4 P_{3/2}) = I(1407.3 \text{ \AA}) / I(1404.7 \text{ \AA})$ while we note that the ratio
 $R_3 = I(2s^2 2p^2 P_{1/2} - 2s 2p^2^4 P_{1/2}) / I(2s^2 2p^2 P_{3/2} - 2s 2p^2^4 P_{5/2}) = I(1399.7 \text{ \AA}) / I(1401.1 \text{ \AA})$ has the same T_e and N_e dependence as R_1 due to common upper levels, but with $R_3 = 1.03 \times R_1$. Similarly, the ratio
 $R_4 = I(2s^2 2p^2 P_{1/2} - 2s 2p^2^4 P_{3/2}) / I(2s^2 2p^2 P_{3/2} - 2s 2p^2^4 P_{3/2}) = I(1397.2 \text{ \AA}) / I(1404.7 \text{ \AA})$ is independent of T_e and N_e due to common upper levels, and has the constant value $R_4 = 0.131$. For S IV, the ratios plotted in Figs 3 and 4 are
 $R_1 = I(3s^2 3p^2 P_{3/2} - 3s 3p^2^4 P_{3/2}) / I(3s^2 3p^2 P_{3/2} - 3s 3p^2^4 P_{5/2}) = I(1416.9 \text{ \AA}) / I(1406.0 \text{ \AA})$ $R_2 = I(3s^2 3p^2 P_{3/2} - 3s 3p^2^4 P_{1/2}) / I(3s^2 3p^2 P_{3/2} - 3s 3p^2^4 P_{3/2}) = I(1423.8 \text{ \AA}) / I(1416.9 \text{ \AA})$ and
 $R_3 = I(3s^2 3p^2 P_{1/2} - 3s 3p^2^4 P_{1/2}) / I(3s^2 3p^2 P_{3/2} - 3s 3p^2^4 P_{5/2}) = I(1404.7 \text{ \AA}) / I(1406.0 \text{ \AA})$. The ratio
 $R_4 = I(3s^2 3p^2 P_{1/2} - 3s 3p^2^4 P_{3/2}) / I(3s^2 3p^2 P_{3/2} - 3s 3p^2^4 P_{5/2}) = I(1398.0 \text{ \AA}) / I(1406.0 \text{ \AA})$ has the same T_e and N_e dependence as R_1 due to common upper levels, but with $R_4 = 0.0492 \times R_1$, while for the same reason the ratios
 $R_5 = I(3s^2 3p^2 P_{1/2} - 3s 3p^2^4 P_{1/2}) / I(3s^2 3p^2 P_{3/2} - 3s 3p^2^4 P_{1/2}) =$

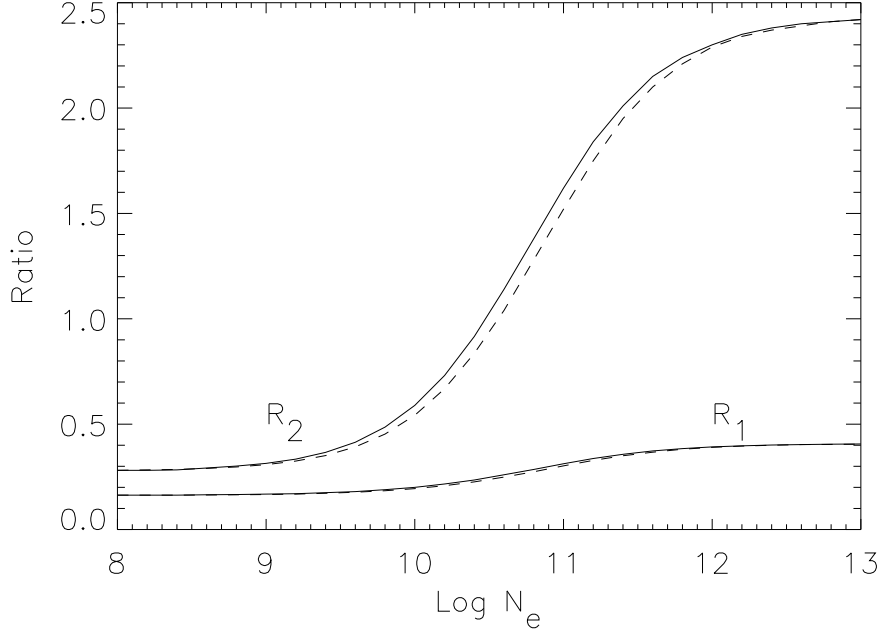


Figure 1. The theoretical O IV line intensity ratios $R_1 = I(2s^22p^2P_{3/2}-2s2p^2^4P_{1/2})/I(2s^22p^2P_{3/2}-2s2p^2^4P_{5/2}) = I(1407.3 \text{ \AA})/I(1401.1 \text{ \AA})$ and $R_2 = I(2s^22p^2P_{3/2}-2s2p^2^4P_{1/2})/I(2s^22p^2P_{3/2}-2s2p^2^4P_{3/2}) = I(1407.3 \text{ \AA})/I(1404.7 \text{ \AA})$, where I is in energy units, plotted as a function of logarithmic electron density (N_e in cm^{-3}) at logarithmic electron temperatures (T_e in K) of $\log T_e = 5.0$ (solid line) and 5.2 (dashed line).

$I(1404.7 \text{ \AA})/I(1423.8 \text{ \AA})$ and $R_6 = I(3s^23p^2P_{1/2}-3s3p^2^4P_{3/2})/I(3s^23p^2P_{3/2}-3s3p^2^4P_{3/2}) = I(1398.0 \text{ \AA})/I(1416.9 \text{ \AA})$ are independent of T_e and N_e and have the constant values $R_5 = 1.37$ and $R_6 = 0.0492$.

We note that the O IV line ratios in Figs 1–4 are very similar (within a few per cent) of those calculated by Harper et al. (1999). However the S IV results differ by up to 30 per cent from those presented by Dufton et al. (1982), due primarily to the adoption of the improved A-value calculations of Hibbert et al. (2002) in the present analysis.

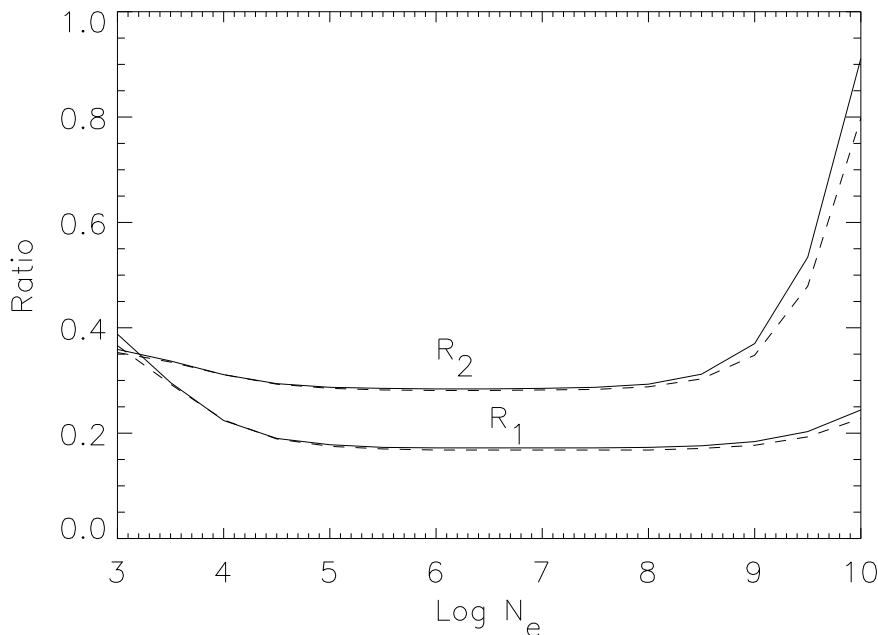


Figure 2. The theoretical O IV line intensity ratios $R_1 = I(2s^22p^2P_{3/2}-2s2p^2^4P_{1/2})/I(2s^22p^2P_{3/2}-2s2p^2^4P_{5/2}) = I(1407.3 \text{ \AA})/I(1401.1 \text{ \AA})$ and $R_2 = I(2s^22p^2P_{3/2}-2s2p^2^4P_{1/2})/I(2s^22p^2P_{3/2}-2s2p^2^4P_{3/2}) = I(1407.3 \text{ \AA})/I(1404.7 \text{ \AA})$, where I is in energy units, plotted as a function of logarithmic electron density (N_e in cm^{-3}) at electron temperatures of $T_e = 10\,000$ K (solid line) and $20\,000$ K (dashed line).

3. OBSERVATIONAL DATA

3.1. HST OBSERVATIONS

HST data of RR Tel were obtained with the *Space Telescope Imaging Spectrograph* (STIS) as part of program 8098 (PI: Keenan). A 2408 s exposure covering the O IV/S IV region (rootname O5EH01010) was taken with the STIS FUV/MAMA and the medium resolution E140M grating on 8 October 2000. The standard 0.2 arc sec square echelle aperture was used, yielding a point source resolution of 1.3 pixels, or 0.021 \AA (4.5 km s^{-1}).

Data were extracted from the archive and re-calibrated using the best available calibration sets available in June 2001. Processing included a correction for scattered light within the echelle instrument, as discussed in the STIS Instrument Handbook Version 5.1. The signal-to-noise per pixel directly measured from the continuum in the processed data for each spectral order near the emission lines of interest is typ-

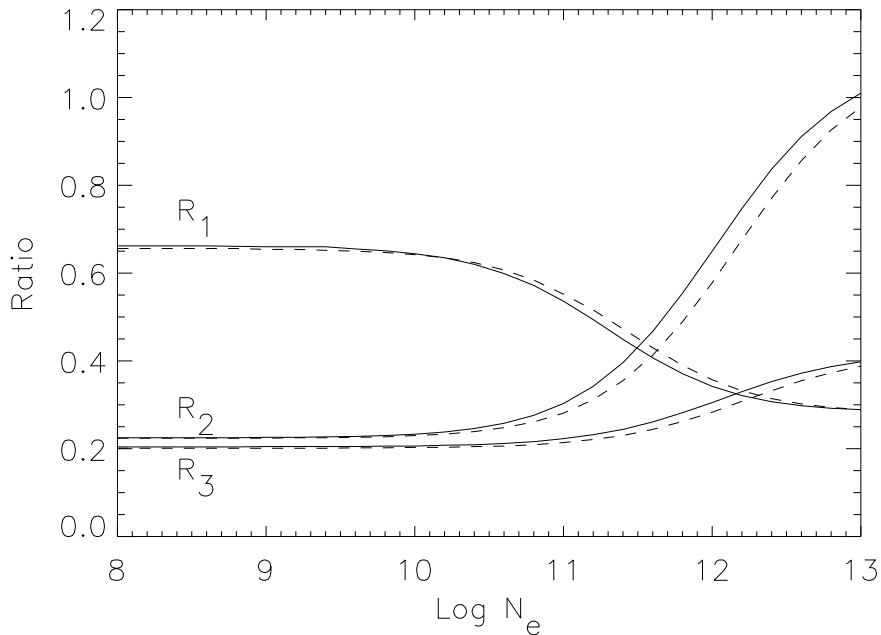


Figure 3. The theoretical S IV line intensity ratios $R_1 = I(3s^23p^2P_{3/2}-3s3p^2^4P_{3/2})/I(3s^23p^2P_{3/2}-3s3p^2^4P_{5/2}) = I(1416.9 \text{ \AA})/I(1406.0 \text{ \AA})$, $R_2 = I(3s^23p^2P_{3/2}-3s3p^2^4P_{1/2})/I(3s^23p^2P_{3/2}-3s3p^2^4P_{3/2}) = I(1423.8 \text{ \AA})/I(1416.9 \text{ \AA})$ and $R_3 = I(3s^23p^2P_{1/2}-3s3p^2^4P_{1/2})/I(3s^23p^2P_{3/2}-3s3p^2^4P_{5/2}) = I(1404.7 \text{ \AA})/I(1406.0 \text{ \AA})$, where I is in energy units, plotted as a function of logarithmic electron density (N_e in cm^{-3}) at logarithmic electron temperatures (T_e in K) of $\log T_e = 5.0$ (solid line) and 5.2 (dashed line).

ically 6–7 per 0.016 Å pixel, and much higher in the emission lines themselves.

In this paper we are interested in the accuracy of the STIS calibration in terms of both flux and wavelength calibration. The STIS Instrument Handbook lists the expected flux accuracy as typically 5 per cent (1σ) for the echelle. However it will be significantly better than this over the limited wavelength range that we are considering (three spectral orders), and also because we are concerned with the relative (rather than the absolute) flux accuracy.

The accuracy of the echelle wavelength calibration has been checked by one of us (BRE) by extracting a long exposure engineering wavecal from the HST archive, taken with the same grating setup. Data obtained for program 8430 as part of the Cycle 8 STIS calibration program in August 2000 (rootname O5J25LXCQ) was used. By modifying the header of these observations, it is possible to calibrate them

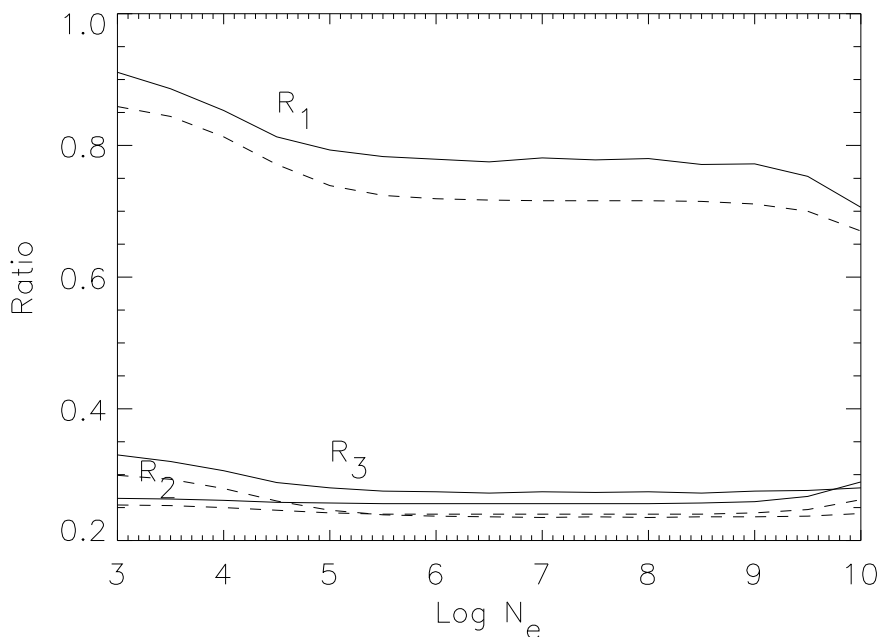


Figure 4. The theoretical S IV line intensity ratios $R_1 = I(3s^23p^2P_{3/2}-3s3p^2^4P_{3/2})/I(3s^23p^2P_{3/2}-3s3p^2^4P_{5/2}) = I(1416.9 \text{ \AA})/I(1406.0 \text{ \AA})$, $R_2 = I(3s^23p^2P_{3/2}-3s3p^2^4P_{1/2})/I(3s^23p^2P_{3/2}-3s3p^2^4P_{3/2}) = I(1423.8 \text{ \AA})/I(1416.9 \text{ \AA})$ and $R_3 = I(3s^23p^2P_{1/2}-3s3p^2^4P_{1/2})/I(3s^23p^2P_{3/2}-3s3p^2^4P_{5/2}) = I(1404.7 \text{ \AA})/I(1406.0 \text{ \AA})$, where I is in energy units, plotted as a function of logarithmic electron density (N_e in cm^{-3}) at electron temperatures of $T_e = 10\,000$ K (solid line) and $20\,000$ K (dashed line).

using CALSTIS, and generate wavelength calibrated spectra. From the measured wavelengths of a sample of known Pt Ne arc lines, the offset between the true and assigned wavelengths can be determined. Details of this approach can be found in STIS Instrument Science Report 98–12, available on the STIS website (<http://www.stsci.edu/hst/stis>). For our calibration dataset, we find an rms scatter of 0.002 \AA , and the relative wavelength scale (Section 4.1) should therefore be accurate to $\pm 0.003 \text{ \AA}$.

In Figs 5 and 6 we show the STIS spectrum of RR Tel between $1390\text{--}1425 \text{ \AA}$, along with identifications of emission features in this wavelength range (see Section 4.1).

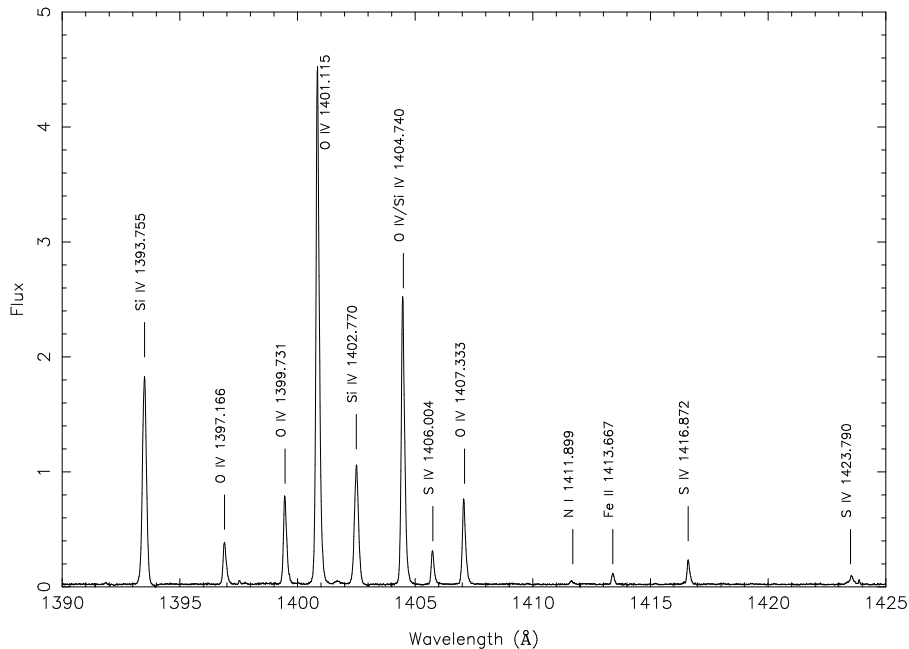


Figure 5. STIS spectrum of RR Telescopii, obtained on 8 October 2000, showing the 1390–1425 Å wavelength range. The flux is in units of 10^{-11} erg cm $^{-2}$ s $^{-1}$ Å $^{-1}$.

3.2. SUMER OBSERVATIONS

The *Solar Ultraviolet Measurements of the Emitted Radiation* (SUMER) instrument on board the *Solar and Heliospheric Observatory* (SoHO) is a high resolution, stigmatic, normal incidence spectrometer covering the wavelength range from 660–1610 Å and 465–805 Å in first and second order, respectively (Wilhelm et al. 1997; Lemaire et al. 1997), with an angular pixel size in the direction along the slit of ~ 1 arc sec and a spectral pixel size between 0.042–0.045 Å. The dataset analysed in this paper was obtained on 18 March 1999, exposing a band of 120 spatial \times 1024 spectral pixels from detector B with a 0.3×120 arc sec slit, positioned through the central part of a sunspot umbra.

In the quiet Sun, all the O IV and S IV lines are weak. However, as shown from *Skylab* data (for example, Doyle et al. 1985), the mid-transition region lines are enhanced over a sunspot umbra, particularly in the plume region. Due to the tilt of the slit, the extraction of spectral lines taken over an extended wavelength region requires proper alignment. For the data considered here, this translated to a ~ 2 arc sec shift between the location of the O IV 1401 Å line compared to the S IV

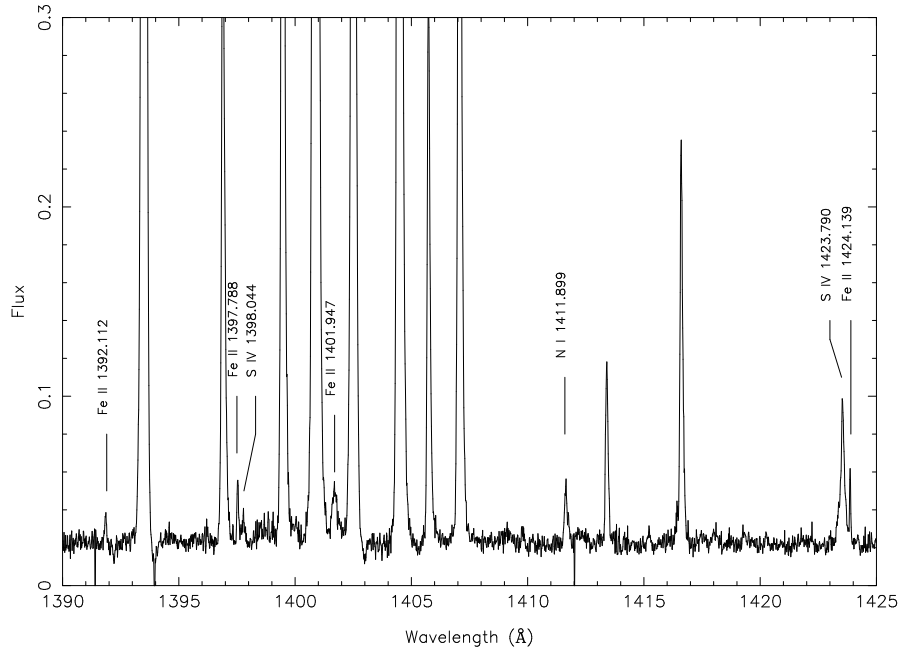


Figure 6. Expanded version of Figure 5, to show weak emission lines.

1423 Å line on detector B. The sunspot plume spectrum analysed here is shown in Figs 7 and 8.

As in the RR Tel spectrum, the SUMER data are affected by blends, in this instance from both first and second order lines. In the SUMER solar spectrum the O IV 1397.22 Å line is blended by Ni II 1397.48 Å (note that the wavelengths given here are those derived from the calibration of Curdt et al. 2001, which differ slightly from the more accurate STIS values). The O IV 1399.77 Å feature is blended in the red wing by Fe II 1399.97 Å, with the contribution of the latter being ~ 40 per cent for the quiet Sun and ~ 20 per cent in a sunspot spectrum. Similarly, O IV 1401.16 Å is affected by a blend with the chromospheric S I 1401.51 Å line. Details about how the degree of blending depends on the solar region observed may be found in Teriaca et al. (2001), but for a sunspot spectrum the S I contribution is only ~ 0.025 per cent. The spectral feature at 1404 Å consists of 3 lines, namely second order O III 702.32 Å at 1404.64 Å, S IV 1404.79 Å and O IV 1404.81 Å. In addition, O IV 1407.39 Å is heavily blended by the second order O III 703.845 and 703.85 Å lines, which appear as one feature at 1407.7 Å and will be referred to as O III 703 Å. This blend can be resolved using a double Gaussian fit and the intensities of both lines can be determined. Since

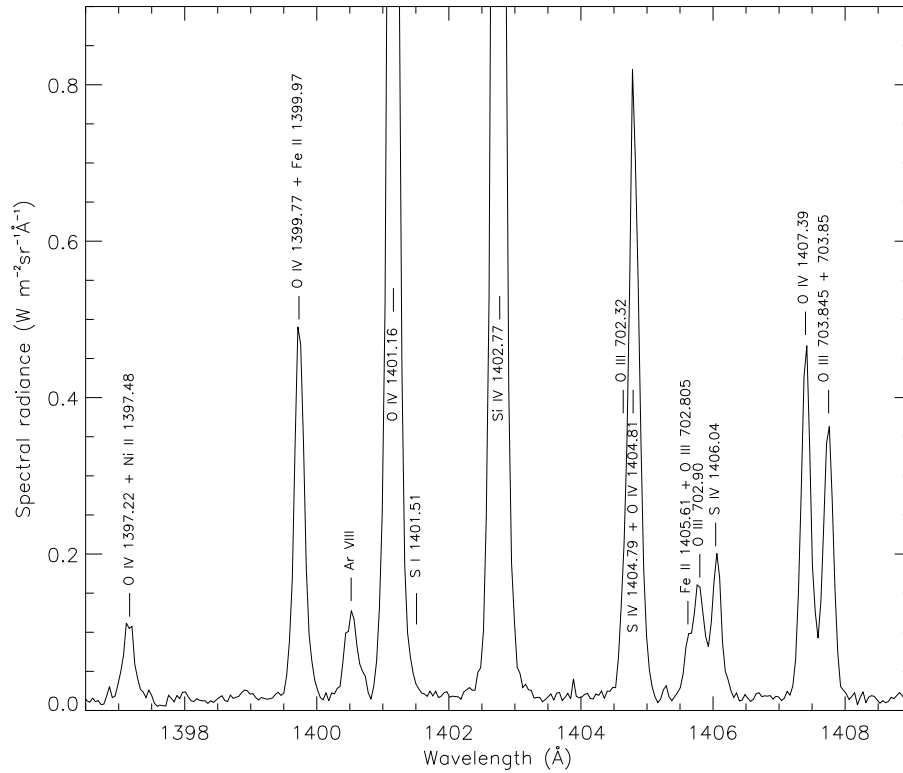


Figure 7. The SUMER sunspot plume spectrum obtained on 18 March 1999 in the 1397–1409 Å wavelength range.

O III 703 Å has the dominant contribution in a quiet Sun spectrum, its parameters are much better determined than those of the O IV line. However, in a sunspot spectrum O IV is stronger and hence its parameters are well determined. Further discussions of O IV blending problems in SUMER spectra may be found in Teriaca et al. and Judge et al. (1998).

The S IV 1406.04 Å line is blended with Fe II 1405.61 Å and second order O III 702.805 and 702.9 Å. Similarly, S IV 1416.93 Å is heavily blended in the blue wing by Fe II 1416.73 Å. The S IV 1423.86 Å line has a strong contribution from Fe II 1424.07 Å, and is sufficiently intense to be selected as a spectral feature only in sunspot observations.

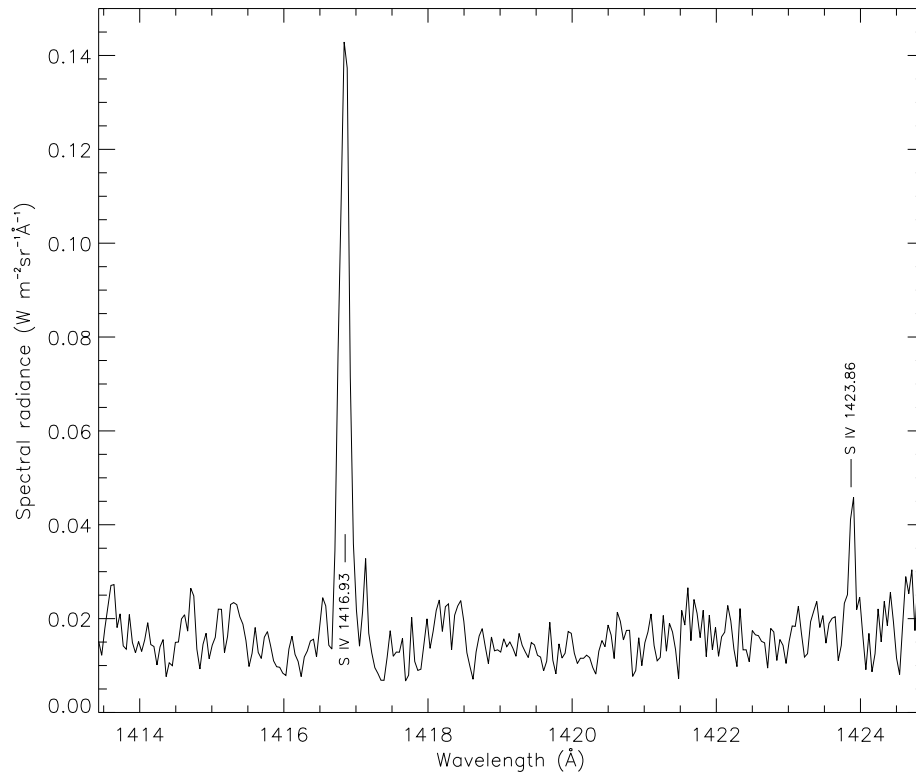


Figure 8. The SUMER sunspot plume spectrum obtained on 18 March 1999 in the 1414–1425 Å wavelength range.

4. RESULTS AND DISCUSSION

4.1. LINE IDENTIFICATIONS, WAVELENGTHS AND ENERGY LEVELS

In Table I we list wavelengths and suggested identifications from the NIST Database at

<http://physics.nist.gov/PhysRefData>

and the Atomic Line List of Peter van Hoof at

<http://www.pa.uky.edu/~peter/atomic>

for the emission features in the RR Tel spectrum between 1392–1425 Å. The rest wavelengths have been derived by shifting the measured values so that the Si IV lines at 1393.755 and 1402.770 Å appear at their rest wavelengths, which have been established to an accuracy of better than ± 0.001 Å (Martin & Zalubas 1983). As noted in Section 3.1, the relative wavelength scale for the RR Tel spectrum should be accurate to ± 0.003 Å, while the error in the wavelength measurements

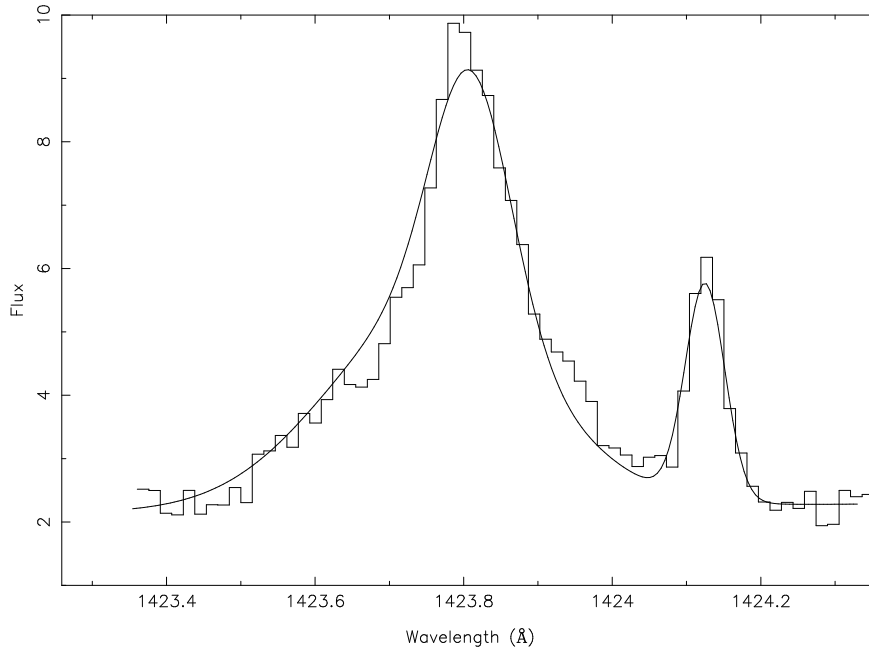


Figure 9. STIS spectrum of RR Telescopii showing the 1423.790 Å feature and the Fe II 1424.139 Å line, where the flux is in units of 10^{-13} erg cm $^{-2}$ s $^{-1}$ Å $^{-1}$. Also plotted is the two component model for the 1423.790 Å line profile, the parameters of which are summarised in Table III.

from the line fitting procedure is less than ± 0.002 Å. Hence the wavelength separation of the features in Table I should be accurate to better than ± 0.004 Å. We discuss our analysis of the O IV and S IV features in this wavelength region separately below.

4.1.1. O IV

The wavelength separation of the O IV 1399.731 and 1407.333 Å lines implies a $2s^22p^2P_{1/2}-2s^22p^2P_{3/2}$ energy difference of 385.91 ± 0.29 cm $^{-1}$. This is identical to the measurement of 385.91 ± 0.29 cm $^{-1}$ obtained from the 1397.166 and 1404.740 Å lines, and is in very good agreement with the value of 385.9 cm $^{-1}$ given by Moore (1983). We note that our wavelength of 1397.166 Å for the $2s^22p^2P_{1/2}-2s2p^2^4P_{3/2}$ line represents a significant improvement over the measurement of 1397.20 Å by Bromander (1969), which could not be determined accurately due to the presence of a blend. In addition, the good agreement found for the $^2P_{1/2}-^2P_{3/2}$ energy separation using the two sets of O IV lines indicates that the measured wavelength of the $2s^22p^2P_{3/2}-2s2p^2^4P_{3/2}$ transition

Table I. Line identifications and fluxes for the RR Tel spectrum.

Wavelength (Å)	FWHM (Å)	Identification	Flux $\pm 3\sigma$ error (erg cm ⁻² s ⁻¹)
1392.112	0.160	Fe II 3d ⁷ b ² F _{5/2} -3d ⁶ 4f ² [2] _{3/2}	(2.47±0.91)×10 ⁻¹⁴
1393.755	0.192	Si IV 3s ² S-3p ² P _{3/2}	(3.63±0.07)×10 ⁻¹²
1397.166	0.153	O IV 2s ² 2p ² P _{1/2} -2s2p ² ⁴ P _{3/2}	(5.59±0.47)×10 ⁻¹³
1397.788	0.069	Fe II 3d ⁶ 4s ² P _{3/2} -3d ⁵ 4s4p ² P _{3/2}	(2.29±0.66)×10 ⁻¹⁴
1398.044	0.069	S IV 3s ² 3p ² P _{1/2} -3s3p ² ⁴ P _{3/2}	(6.74±4.41)×10 ⁻¹⁵
1399.731	0.155	O IV 2s ² 2p ² P _{1/2} -2s2p ² ⁴ P _{1/2}	(1.20±0.08)×10 ⁻¹²
1401.115	0.161	O IV 2s ² 2p ² P _{3/2} -2s2p ² ⁴ P _{5/2}	(7.27±0.41)×10 ⁻¹²
1401.947	0.160	Fe II 3d ⁶ 4s ⁴ D _{7/2} -3d ⁵ 4s4p ⁶ P _{5/2}	(3.79±0.83)×10 ⁻¹⁴
1402.770	0.196	Si IV 3s ² S-3p ² P _{1/2}	(2.09±0.05)×10 ⁻¹²
1404.740	0.161	O IV 2s ² 2p ² P _{3/2} -2s2p ² ⁴ P _{3/2} + S IV 3s ² 3p ² P _{1/2} -3s3p ² ⁴ P _{1/2}	(4.10±0.27)×10 ⁻¹²
		O IV 2s ² 2p ² P _{3/2} -2s2p ² ⁴ P _{3/2}	(3.91±0.31)×10 ⁻¹² ^a
1406.004	0.135	S IV 3s ² 3p ² P _{3/2} -3s3p ² ⁴ P _{5/2}	(4.05±0.27)×10 ⁻¹³
1407.333	0.155	O IV 2s ² 2p ² P _{3/2} -2s2p ² ⁴ P _{1/2}	(1.15±0.08)×10 ⁻¹²
1411.899	0.160	N I 2s ² 2p ³ ² P-2s ² 2p ² 3s ² D	(4.56±0.91)×10 ⁻¹⁴
1413.667	0.128	Fe II 3d ⁶ 4s ⁴ H _{11/2} -3d ⁵ 4s4p ⁴ H _{11/2}	(1.25±0.17)×10 ⁻¹³
1416.872	0.126	S IV 3s ² 3p ² P _{3/2} -3s3p ² ⁴ P _{3/2}	(2.61±0.41)×10 ⁻¹³
1423.790	0.213	S IV 3s ² 3p ² P _{3/2} -3s3p ² ⁴ P _{1/2}	(1.38±0.24)×10 ⁻¹³
1424.139	0.063	Fe II 3d ⁶ 4s ⁴ P _{5/2} -3d ⁶ 5p ⁴ D _{3/2}	(2.19±0.94)×10 ⁻¹⁴

^aCorrected for presence of S IV line (see Section 4.2 for details).

at 1404.740 Å is not affected by the presence of the S IV 3s²3p²P_{1/2}-3s3p²⁴P_{1/2} line, as also implied by the line intensity ratio analysis (see Section 4.2).

The wavelength separation of the 1397.166 and 1399.731 Å line pair, and 1404.740 plus 1407.333 Å transitions, imply a 2s2p²⁴P_{1/2}-2s2p²⁴P_{3/2} energy difference of 131.16±0.29 and 131.16±0.29 cm⁻¹, respectively. These are in excellent agreement, although 0.86 cm⁻¹ greater than the value of 130.3 cm⁻¹ given by Moore (1983). Similarly, the wavelengths of the 1401.115 and 1404.740 Å features indicate a 2s2p²⁴P_{3/2}-2s2p²⁴P_{5/2} energy separation of 184.18±0.29 cm⁻¹, compared with the Moore estimate of 185.4 cm⁻¹. Given the internal consistency of our results, we believe that our energy levels are to be preferred over those of Moore. The values for the 2s2p²⁴P energy levels clearly require further investigation in the laboratory, as also suggested by Harper et al. (1999).

Table II. O IV and S IV line ratios in the RR Tel spectrum.

Species	Ratio designation	Observed value	Theory ^a
O IV	R ₁	0.16±0.01	0.17
O IV	R ₂	0.29±0.03	0.28
O IV	R ₃	0.17±0.01	0.18
O IV	R ₄	0.14±0.02	0.13
S IV	R ₁	0.64±0.11	0.72
S IV	R ₂	0.53±0.12	0.24
S IV	R ₂	0.20±0.08 ^b	0.24
S IV	R ₄	0.017±0.011	0.035
S IV	R ₆	0.026±0.017	0.049

^aCalculated at $T_e = 20\,000$ K and $N_e = 10^6$ cm⁻³.

^bEstimated using revised S IV $3s^23p^2P_{3/2}-3s3p^2^4P_{1/2}$ line intensity from Table III (see Section 4.2 for details).

Table III. Parameters of the two component model for the 1423.790 Å line profile in RR Tel.

Wavelength (Å)	FWHM (Å)	Identification	Flux ± 3σ error (erg cm ⁻² s ⁻¹)
1423.774	0.333	S VI 4d ² D _{3/2} -5p ² P _{1/2} ?	(1.12±0.39)×10 ⁻¹³
1423.824	0.126	S IV 3s ² 3p ² P _{3/2} -3s3p ² ⁴ P _{1/2}	(5.29±1.88)×10 ⁻¹⁴

Table IV. O IV and S IV line intensities in the SUMER sunspot spectrum.

Transition	FWHM (Å)	Flux ± 3σ error (W m ⁻² sr ⁻¹)
O IV 1401.16 Å	0.140	2.19±0.16
S IV 1406.04 Å	0.137	0.183±0.052
O IV 1407.39 Å	0.151	0.453±0.074
S IV 1416.93 Å	0.126	0.134±0.024
S IV 1423.86 Å	0.055	0.033±0.025

4.1.2. S IV

The wavelength separation of the 1398.044 and 1416.872 Å lines implies a $3s^23p^2P_{1/2}-3s^23p^2P_{3/2}$ interval of $950.50±0.29$ cm⁻¹, in reasonable agreement with the Kaufman & Martin (1993) value of 951.43 cm⁻¹.

Table V. O IV and S IV line ratios in the SUMER sunspot spectrum.

Species	Ratio designation	Observed value	Derived density or theoretical value
O IV	R ₁	0.21±0.04	10.2±0.4 ^a
S IV	R ₁	0.73±0.25	0.64 ^b
S IV	R ₂	0.25±0.19	0.24 ^b

^aFor O IV we list the derived value of $\log N_e$ (N_e in cm^{-3}), using the calculations in Figure 1 at $\log T_{max} = 5.2$ (Mazzotta et al. 1998).

^bFor S IV we list the theoretical ratios from Figure 3, using the calculations for $\log T_{max} = 5.0$ (Mazzotta et al. 1998) and $\log N_e = 10.2$.

This provides support for the identification of the line at 1398.044 Å being due to the S IV $3s^23p^2P_{1/2}-3s3p^2^4P_{3/2}$ transition, which is also indicated from a line intensity ratio analysis (see Section 4.2). This confirms the tentative detection of this line in the solar spectrum by Curdt et al. (2001), and is the first time (to our knowledge) that this feature has been observed in an astrophysical source other than the Sun. In addition, our wavelength determination represents an improvement over the value of 1398.06 Å measured by Curdt et al. from SUMER data.

The 1416.872 and 1423.790 Å transitions imply a $3s3p^2^4P_{1/2}-3s3p^2^4P_{3/2}$ interval of $342.93\pm0.29 \text{ cm}^{-1}$, in poor agreement with the Kaufman & Martin (1993) result of 344.6 cm^{-1} . However we note that a consideration of line ratios involving the 1423.790 Å feature indicates possible blending, and hence the wavelength of this line may be ill-determined (see Section 4.2). From the 1406.004 and 1416.872 Å transitions, we find a $3s3p^2^4P_{3/2}-3s3p^2^4P_{5/2}$ separation of $545.55\pm0.29 \text{ cm}^{-1}$, in good agreement with the Kaufman & Martin value of 545.69 cm^{-1} .

The measured wavelength of the 1423.790 Å line and the $3s^23p^2P_{1/2}-3s^23p^2P_{3/2}$ interval of 950.50 cm^{-1} implies that the $3s^23p^2P_{1/2}-3s3p^2^4P_{1/2}$ feature should lie at 1404.779 Å. This is in better agreement with the Kelly (1987) wavelength of 1404.77 Å than the Kaufman & Martin (1993) value of 1404.808 Å, and would appear to indicate that this line is more closely blended with the O IV 1404.740 Å transition than previously thought. However as noted above the 1423.790 Å wavelength measurement is not secure, and hence little weight should be attached to any prediction of the S IV $3s^23p^2P_{1/2}-3s3p^2^4P_{1/2}$ line wavelength. In any event, this feature contributes at most a few per cent to the O IV/S IV 1404.7 Å line blend (see Section 4.2).

4.2. O IV AND S IV LINE INTENSITY RATIOS IN RR TEL

The full-width half maximum (FWHM) line widths and intensities of the emission features in the RR Tel spectrum, measured using the spectrum synthesis package DIPSO (Howarth, Murray & Mills 1994), are summarised in Table I, along with the 3σ errors in the latter. Resultant values of the ratios R_1 through R_4 (O IV) and R_1 through R_6 (S IV) are listed in Table II. The theoretical S IV ratio $R_5 = I(1404.7 \text{ \AA})/I(1423.8 \text{ \AA}) = 1.37$ (Section 2) has been used in conjunction with the measured 1423.8 \AA line flux to determine the contribution of the S IV component to the O IV/S IV 1404.7 \AA blend. We find that S IV contributes less than 5 per cent to the total 1404.7 \AA line flux, and hence has a negligible effect on the derived R_2 and R_4 line ratios in O IV. Indeed, further analysis indicates that the S IV contribution may be even smaller (see below).

Diagnostic line ratios in other species in the RR Tel spectrum, ranging from Al II to O V, indicate an electron temperature close to 20 000 K and electron densities $N_e \simeq 10^5\text{--}10^8 \text{ cm}^{-3}$ (Keenan et al. 1994, 1999, 2002; McKenna et al. 1997; Hayes & Nussbaumer 1986). Over this temperature and density interval, the predicted O IV and S IV line ratios are effectively constant (see Figs 3 and 4), and in Table 2 we therefore list their theoretical values at $T_e = 20\,000 \text{ K}$ and $N_e = 10^6 \text{ cm}^{-3}$. However we note that varying the temperature by a factor of two and the density by several orders of magnitude leads to a < 10 per cent change in the theoretical line ratios, and hence would not alter the discussion presented below.

An inspection of Table II reveals excellent agreement between theory and observation for all of the O IV line ratios. In the case of S IV there is generally good agreement for R_1 , R_4 and R_6 (taking into account the 15 per cent uncertainty in the theoretical results as well as the observational errors), with the latter providing additional support for the identification of the 1398.044 \AA feature being due to the S IV $3s^23p^2P_{1/2}\text{--}3s3p^2^4P_{3/2}$ transition. However the observed value of R_2 is about a factor of two larger than theory predicts, probably due to blending in the 1423.790 \AA line. Additional support for blending of this feature comes from the line width, which we can see from Table I is somewhat larger than for the other S IV features. A closer inspection of the line profile, shown in Fig. 9, also suggests a possible asymmetry.

We have therefore fitted the 1423.790 \AA line profile using a two component model, shown in Fig. 9 and summarised in Table III. For one component, we fixed the wavelength to that predicted for the S IV $3s^23p^2P_{3/2}\text{--}3s3p^2^4P_{1/2}$ transition (1423.824 \AA), obtained from the measured $3s^23p^2P_{3/2}\text{--}3s3p^2^4P_{3/2}$ value (1416.872 \AA) in conjunction

with the Kaufman & Martin (1993) $3s3p^2\ ^4P_{1/2}$ – $3s3p^2\ ^4P_{3/2}$ separation of $344.6\ \text{cm}^{-1}$. In addition, we set the FWHM for the $1423.824\ \text{\AA}$ component to that measured for the S IV $1416.872\ \text{\AA}$ line, i.e. $0.126\ \text{\AA}$.

The resultant measured intensity of the $1423.824\ \text{\AA}$ line implies a revised $R_2 = 0.20 \pm 0.08$, in good agreement with the theoretical value of 0.24. In addition, this new intensity measurement indicates that the S IV $3s^23p\ ^2P_{1/2}$ – $3s3p^2\ ^4P_{1/2}$ transition makes a smaller contribution to the O IV/S IV $1404.7\ \text{\AA}$ blend than previously thought (see above), of less than 2 per cent.

The second component of the $1423.790\ \text{\AA}$ feature has a rest wavelength of $1423.774\ \text{\AA}$ and a FWHM of $0.333\ \text{\AA}$. Crawford (2000) has noted a correlation between the FWHM of an emission line in the RR Tel spectrum and the ionization potential (IP) of the relevant species. The FWHM – IP relationship derived by this author implies that the IP of the ion responsible for the $1423.774\ \text{\AA}$ line is ~ 80 – $120\ \text{eV}$. An inspection of the NIST Database and the Atomic Line List reveals the only likely candidate to be a S VI line at $1423.846\ \text{\AA}$, although we note that this is predicted to lie on the long wavelength side of the S IV feature, and not shortward as indicated by the present analysis. Clearly a further investigation of this wavelength region is highly desirable, both to improve on wavelength measurements and identify blending species.

We note in passing that Keenan et al. (1993) have measured O IV line ratios in an RR Tel spectrum obtained with the *International Ultraviolet Explorer* (IUE) satellite. However the IUE observations are not of as high a quality as the HST data presented here, although they are in good agreement with the line ratio calculations in Fig. 2, with discrepancies between theory and experiment of less than 30 per cent.

4.3. O IV AND S IV LINES IN THE SUMER SUNSPOT SPECTRUM

Cook et al. (1995) found very poor agreement between theory and observation for the S IV line ratios from *Skylab* S082B and *High Resolution Telescope and Spectrograph* (HRTS) solar spectra, and also for HST/*Goddard High Resolution Spectrograph* (GHRS) observations of the binary star Capella. In addition, the electron densities derived from the S IV diagnostics differed by large factors (> 10) from those estimated using O IV line ratios. These discrepancies were probably due to blending in the observations, especially for the solar spectra, which were recorded on photographic emulsions and hence of relatively poor signal-to-noise.

Brage et al. (1996) suggested that an analysis of high quality SUMER data would allow blending problems in the O IV/S IV spectral region

to be clarified. However both the O IV and S IV lines in SUMER spectra are affected by blends, from first and/or second order lines, as detailed in Section 3.2.

Where possible, we have measured O IV and S IV line intensities in the SUMER sunspot spectrum using the CFIT procedure from the solar software, employing profile fitting techniques to remove the effects of blends by other first and/or second order lines. These intensities are listed in Table IV, along with the 3σ errors and line widths, while the resultant O IV and S IV line ratios are summarised in Table V. An inspection of this table reveals excellent agreement between the observed S IV line ratios and the theoretical values calculated at an electron density appropriate to the O IV emitting region of the sunspot plasma, namely $N_e = 10^{10.2} \text{ cm}^{-3}$. This resolves discrepancies previously found between O IV and S IV line ratios by Cook et al. (1995), as discussed above. Clearly however, better quality solar spectra covering the O IV/S IV wavelength range would be highly desirable, to reliably measure and assess all lines.

ACKNOWLEDGEMENTS

KME and MSM are grateful to PPARC for financial support, while SA acknowledges the award of a postgraduate studentship from the Department of Employment and Learning for Northern Ireland. Research at Armagh Observatory is grant-aided by the Department of Culture, Arts and Leisure for Northern Ireland. The RR Tel observations were made with the NASA/ESA Hubble Space Telescope at STScI which is operated by the Association of Universities for Research in Astronomy, Inc. under NASA contract NAS 5-26555. The SUMER project is financially supported by DLR, CNES, NASA, and PRODEX. We thank W. Curdt for helpful discussions, and P. van Hoof for use of his Atomic Line List.

REFERENCES

- Bhatia A. K., Doschek G. A., Feldman U., 1980, A&A, 86, 32
 Brage T., Judge P. G., Brekke P., 1996, ApJ, 464, 1030
 Bromander J., 1969, Ark. Fys., 40, 257
 Cook J. W., Keenan F. P., Dufton P. L., Kingston A. E., Pradhan A. K., Zhang H. L., Doyle J. G., Hayes M. A., 1995, ApJ, 444, 936
 Crawford F. L., 2000, PhD Thesis, Queen's University of Belfast
 Curdt W., Brekke P., Feldman U., Wilhelm K., Dwivedi B. N., Schühle U., Lemaire P., 2001, A&A, 375, 591
 Dankwort W., Treffitz E., 1978, A&A, 65, 93

- Doyle J.G., Raymond J.C., Noyes R.W., Kingston A.E., 1985, *ApJ* 297, 816
- Dufton P. L., 1977, *Comput. Phys. Commun.*, 13, 25
- Dufton P.L., Berrington K.A., Burke P.G., Kingston A.E., 1978, *A&A*, 62, 111
- Dufton P.L., Hibbert A., Kingston A.E., Doschek G.A., 1982, *ApJ*, 257, 338
- Feldman U., Behring W. E., Curdt W., Schühle U., Wilhelm K., Lemaire P., Moran T. M., 1997, *ApJS*, 113, 195
- Flower D.R., Nussbaumer H., 1975, *A&A*, 45, 145
- Foster V. J., Keenan F. P., Reid R. H. G., 1996, *A&A*, 308, 1009
- Foster V. J., Reid R. H. G., Keenan F. P., 1997, *MNRAS*, 288, 973
- Harper G. M., Jordan C., Judge P. G., Robinson R. D., Carpenter K. G., Brage T., 1999, *MNRAS*, 303, L41
- Hayes M. A., Nussbaumer H., 1986, *A&A*, 161, 287
- Hibbert A., Brage T., Fleming J., 2002, *MNRAS*, 333, 885
- Howarth I. D., Murray J., Mills D., 1994, *Starlink User Note No.* 50.15
- Johnson C. T., Kingston A. E., Dufton P. L., 1986, *MNRAS*, 220, 155
- Judge P. G., Hansteen V., Wikstøl Ø., Wilhelm K., Schühle U., Moran T., 1998, *ApJ*, 502, 981
- Kaufman V., Martin W. C., 1993, *J. Phys. Chem. Ref. Data*, 22, 279
- Keenan F. P., Aller L. H., Espey B. R., Exter K. M., Hyung S., Keenan M. T. C., Pollacco D. L., Ryans R. S. I., 2002, *Proc. Natl. Acad. Sci. USA*, 99, 4152
- Keenan F. P., Conlon E. S., Bowden D. A., Feibelman W. A., Pradhan A. K., 1993, *ApJS*, 88, 169
- Keenan F. P., Dufton P. L., Feibelman W. A., Bell K. L., Hibbert A., Stafford R. P., 1994, *ApJ*, 423, 882
- Keenan F. P., Espey B. R., Mathioudakis M., Aggarwal K. M., Crawford F. L., Feibelman W. A., McKenna F. C., 1999, *MNRAS*, 309, 195
- Kelly R. L., 1987, *J. Phys. Chem. Ref. Data*, 16, Suppl. 1
- Lemaire P., Wilhelm K., Curdt W., Schühle U., Marsch E., Poland A. I., et al., 1997, *Solar Phys*, 170, 105
- McKenna F. C., Keenan F. P., Aller L. H., Hyung S., Feibelman W. A., Berrington K. A., Fleming J., Hibbert A., 1997, *ApJ*, 486, 571
- Martin W. C., Zalubas R., 1983, *J. Phys. Chem. Ref. Data*, 12, 323
- Martin W. C., Zalubas R., Musgrove A., 1990, *J. Phys. Chem. Ref. Data*, 19, 821

- Mazzotta P., Mazzitelli G., Colafrancesco S., Vittorio N., 1998, A&AS, 133, 403
- Moore C.E., 1983, Natl. Stand. Ref. Data Ser., 3, 10
- Nussbaumer H., Storey P. J., 1982, A&A, 115, 205
- Safronova M. S., Johnson W. R., Safronova U. I., 1996, Phys. Rev. A, 54, 2850
- Tayal S. S., 2000, ApJ, 530, 1091
- Teriaca L., Madjarska M. S., Doyle J.G., 2001, Solar Phys., 200, 91
- Wilhelm K., Lemaire P., Curdt W., Schühle E., Marsch E., Poland A. I., et al., 1997, Solar Phys., 170, 75
- Zhang H. L., Graziani M., Pradhan A. K., 1994, A&A, 283, 319